NASA TECHNICAL MEMORANDUM

NASA TM X-888

NASA TM X-888

STUDY OF THE EFFECTS OF A ROCKET EXHAUST ON RADIO FREQUENCY SIGNAL ATTENUATION BY THE USE OF A RECOVERABLE CAMERA ON THE NASA SCOUT VEHICLE

By Duncan E. McIver, Jr.
Langley Research Center
Langley Station, Hampton, Va.

NATIONAL AERONAUTICS AND SPACE ADMINISTRATION • WASHINGTON, D. C. • OCTOBER 1963

~~CONFIDENTIAL~~
UNCLASSIFIED

TECHNICAL MEMORANDUM X-888

STUDY OF THE EFFECTS OF A ROCKET EXHAUST ON RADIO FREQUENCY SIGNAL ATTENUATION BY THE USE OF A RECOVERABLE CAMERA ON THE NASA SCOUT VEHICLE

By Duncan E. McIver, Jr.

Langley Research Center
Langley Station, Hampton, Va.

NATIONAL AERONAUTICS AND SPACE ADMINISTRATION

UNCLASSIFIED
~~CONFIDENTIAL~~

NATIONAL AERONAUTICS AND SPACE ADMINISTRATION

TECHNICAL MEMORANDUM X-888

STUDY OF THE EFFECTS OF A ROCKET EXHAUST ON RADIO FREQUENCY SIGNAL ATTENUATION BY THE USE OF A RECOVERABLE CAMERA ON THE NASA SCOUT VEHICLE*

By Duncan E. McIver, Jr.

SUMMARY

A recoverable camera was flown on a NASA Scout vehicle to photograph the exhaust of the solid-propellant second-stage rocket motor during an anticipated period of unusual VHF signal attenuation which had been observed on previous Scout launches. The recovered film reveals the formation of a luminous "ring" on the periphery of the exhaust coincident with the onset of pronounced attenuation. The ring formation occurred at 181,000 feet (second-stage ignition occurred at 131,500 feet) and continued until motor tail off at 225,000 feet. A portion of the ring disappeared during hydrogen peroxide control jet actuation and coincided with relief from observed signal attenuation.

The Wallops launch site tracking station recorded a 20-decibel attenuation on all three telemetry signals, whereas the Langley station, at a larger vehicle-to-tracking-station aspect angle (50°), recorded a 5-decibel enhancement on two of the signals and a 20-decibel attenuation on the third. Onboard measurements of two of the antenna systems revealed that the voltage standing wave ratio did not change during the attenuation period. Analysis of the data indicates: (1) the luminous ring is afterburning on the exhaust surface due to an interaction with the vehicle flow field; (2) electrons created by ionization processes in the afterburning sheath cause attenuation and reflection of radio frequency energy; (3) the control jets quench the afterburning and signal recovery occurs; (4) the observed attenuation can be explained in terms of an effective change in vehicle antenna patterns; and (5) the lack of change in voltage standing wave ratio indicates that antenna breakdown did not occur.

INTRODUCTION

The exhaust free jet (plume) of present-day solid-propellant rocket boosters can severely attenuate radio signals and create serious range safety and data acquisition problems. (See refs. 1 to 3.) The exhausts contain free electrons

*Title, Unclassified.

which absorb and reflect electromagnetic energy. These electrons are usually created in the combustion chamber and exit with the combustion gases. At high altitudes the exhaust expands to intercept the line of sight between the vehicle antennas and the tracking stations and signal loss occurs. Electron density on the surface of the exhaust is increased if afterburning occurs. Although it is generally possible to employ down-range tracking stations which do not "look through" the exhaust, this technique is not always practical.

Other approaches to the problem include changes in propellant composition and changes in communication-link frequencies. The former, which is designed to reduce the electron level chemically, would be difficult for existing operational vehicles but seems to be a reasonable approach for prospective booster systems. The latter approach is pursued since, in general, higher radio frequencies suffer less attenuation; however, flight results (refs. 2 and 3) reveal that frequencies as high as 5,000 megacycles have suffered severe attenuation and anticipated increases in propellant performance should aggravate the problem.

A different approach to the problem was revealed when the first Scout was launched from Wallops Island, Virginia, in July 1960. (See ref. 1.) During this launch, the second stage ignited at 130,000 feet. Several seconds later, at a vehicle altitude of 197,000 feet, the launch-site tracking station recorded an attenuation of telemetry signals which continued to motor tail off at 260,000 feet. However, each time the hydrogen peroxide control jets fired, the attenuation was removed. Analysis indicated that the introduction of a small amount of material (1/70th of second-stage motor mass flow) on the surface of the exhaust was effective in eliminating exhaust-induced signal interference.

The Langley Research Center is continuing its investigation of the attenuation-recovery phenomenon of the Scout second-stage rocket motor. This report presents the results of a flight camera experiment, flown on Scout ST-8 launched from Wallops Island, Virginia, shortly after midnight on March 1, 1962, in which the second-stage exhaust was filmed from ignition to burnout.

THE SCOUT VEHICLE

The Scout vehicle which carried the camera experiment is shown in figures 1 and 2. Although the boost system for this vehicle employed five solid-propellant rocket motors, the motor of interest to this presentation is the second stage. The Castor second-stage motor has a relatively high aluminized composite-type propellant developing 60,000 pounds thrust. Other motor data, including exhaust gas composition, are shown in table I and discussed in reference 4.

Two pitch and two yaw motors, located near the second-stage motor nozzle, are used for attitude control. Thrust from these motors is directed normal to the vehicle axis and is generated by the rapid decomposition of hydrogen peroxide creating a nominal mass flow of 3.5 pounds per second. Important characteristics of the control jets are given in table II; additional information is contained in reference 4.

TABLE I.- NOMINAL DATA ON SCOUT SECOND-STAGE ROCKET MOTOR

[Manufactured by Thiokol Chemical Corporation]

Propellant weight, lb	7,320
Propellant composition:	
Aluminum, percent by weight	14
Ammonium perchlorate, percent by weight	65
Polybutyldiene acrylic acid, percent by weight	21
Chamber pressure, lb/sq in. abs	520
Combustion (chamber) temperature, ^{o}F	5,225
Ratio of specific heats, γ	1.18
Throat diameter, in.	9.69
Exit diameter, in.	38.5
Divergence angle of nozzle, deg	20.66
Exit pressure, lb/sq in. abs	4
Gas (exit) temperature, ^{o}F	2,580
Exit density, lb/cu ft	0.00328
Exit Mach number	3.41
Thrust, lb	60,000
Mass flow (First 27 sec), lb/sec	240
Exhaust gas composition (Manufacturer's specification):	
Al_2O_3, percent by weight	26
CO, percent by weight	27
H_2O, percent by weight	9
H_2, percent by weight	3
N_2, percent by weight	8
HCl, percent by weight	22
CO_2, percent by weight	5

TABLE II.- SECOND-STAGE PITCH AND YAW HYDROGEN PEROXIDE JET CHARACTERISTICS

Propellant	90% pure hydrogen peroxide
Chamber pressure, lb/sq in. abs	300 to 400
Adiabatic (chamber) decomposition temperature, ^{o}F	1,354
Exit temperature, ^{o}F	400
Exit velocity, ft/sec	4,100
Thrust, lb	500
Mass flow rate, lb/sec	3.5
Exhaust composition:	
Water vapor, percent by weight	60
Oxygen, percent by weight	40
Normal on-time, sec	0.1

Decomposition process: Hydrogen peroxide is passed through a silver screen catalyst bed and converted to water vapor and oxygen.

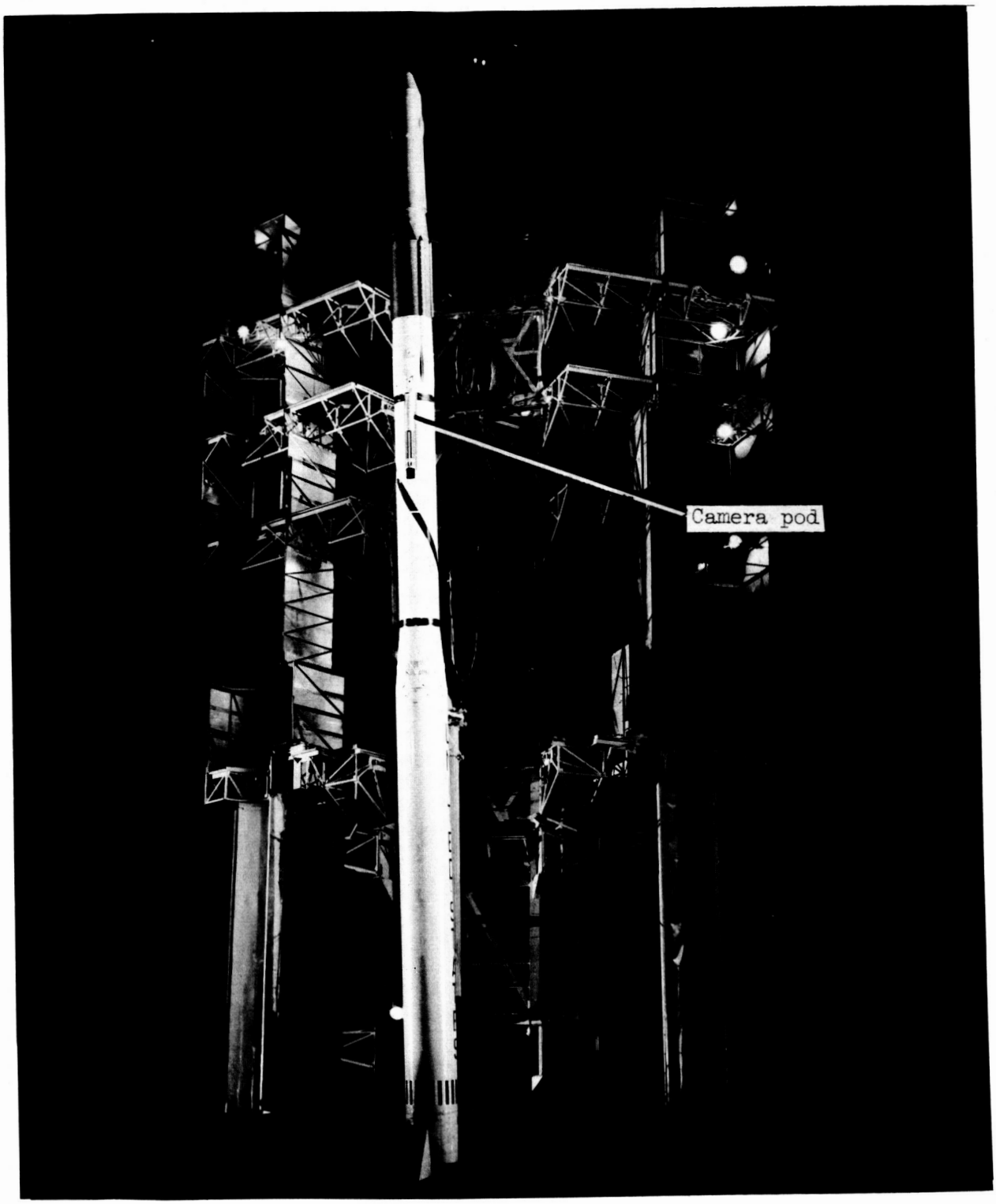

Figure 1.- Scout ST-8 with "piggyback" camera installed. L-62-944.1

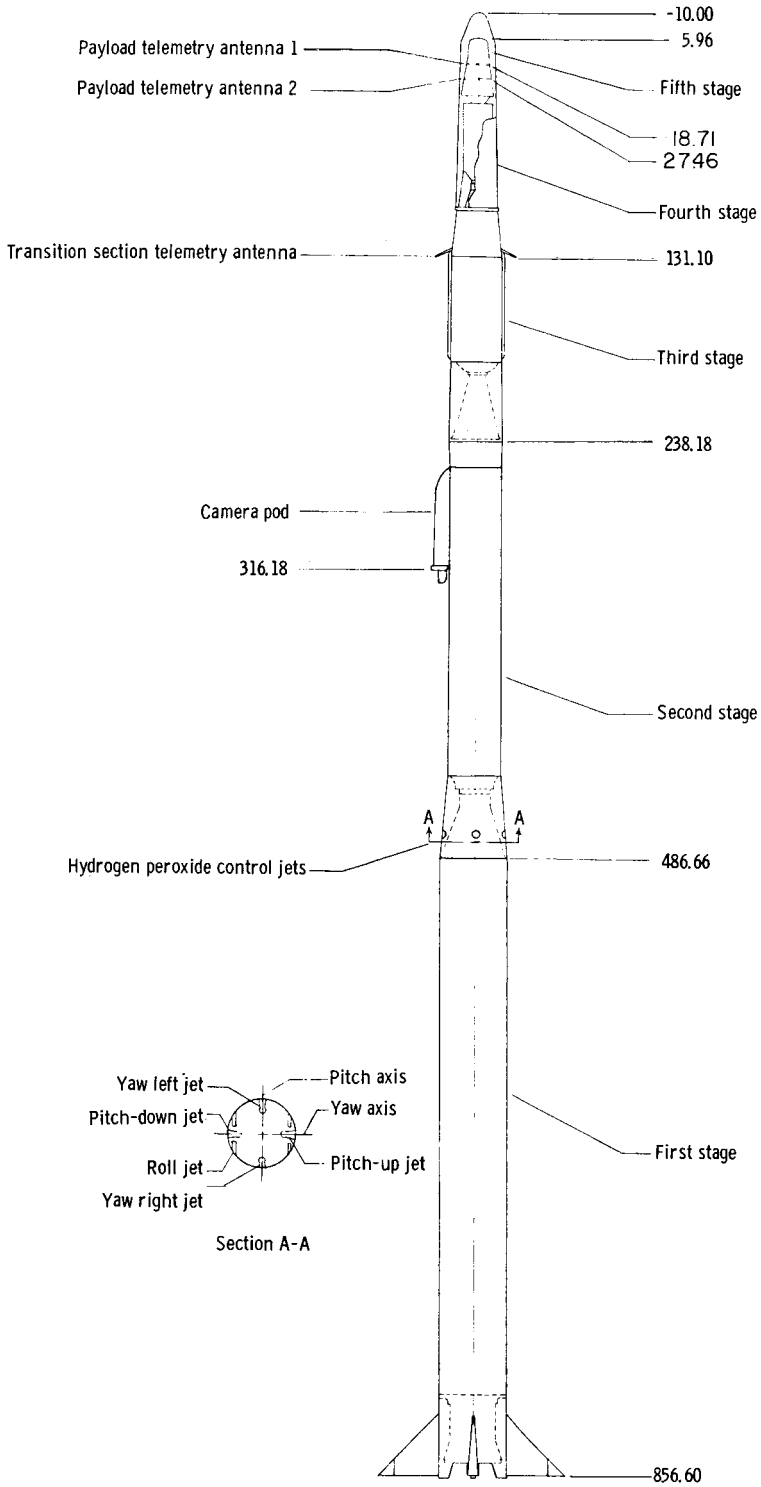

Figure 2.- Scout vehicle used to carry the camera experiment.

Figure 3.- ST-8 payload telemetry antenna patterns.

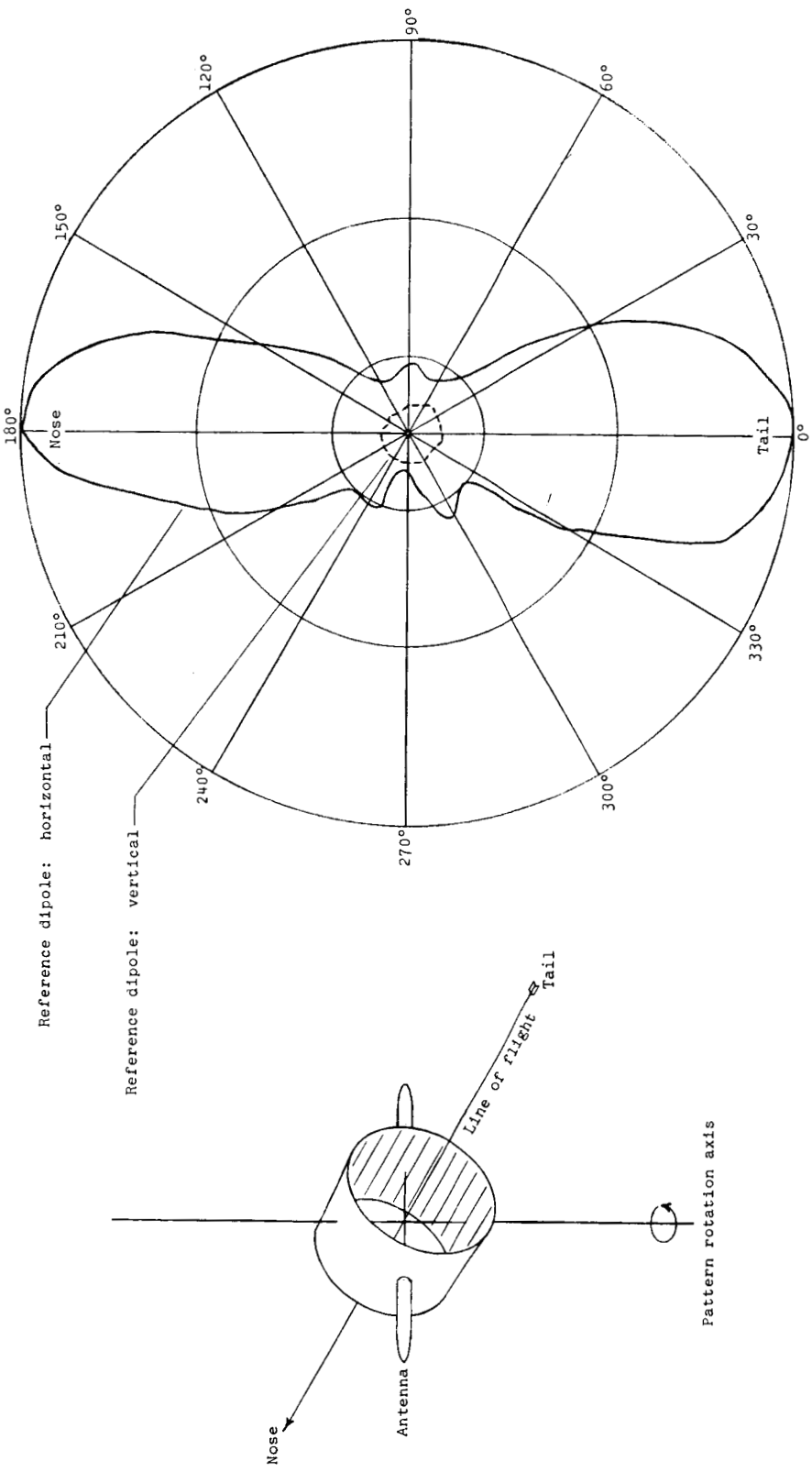

Figure 4.- ST-8 transition section telemetry antenna pattern.

INSTRUMENTATION

Three separate VHF telemetry systems were employed on the launch vehicle: Two in the payload and a third in the transition (adapter) section between the third and fourth stages. The locations of the antennas are shown in figure 2. Signal frequencies, transmitter powers, and antenna types are listed in table III and antenna radiation patterns are shown in figures 3 and 4.

TABLE III.- TELEMETRY SYSTEMS

System	Frequency, Mc	Power, watts	Antenna
Payload telemeter 1	225.7	10	Ring
Payload telemeter 2	240.2	10	Ring
Transition section telemeter	244.3	10	Dipole spikes

Directional couplers were placed in the transmission lines of both payload antennas to monitor and telemeter the VSWR (voltage standing wave ratio). This antenna monitoring system is described in reference 5.

The two ground tracking stations previously mentioned recorded signal strength and telemetry data from the vehicle for correlation with the film. Figure 5 shows the orientation of the tracking stations with respect to the vehicle

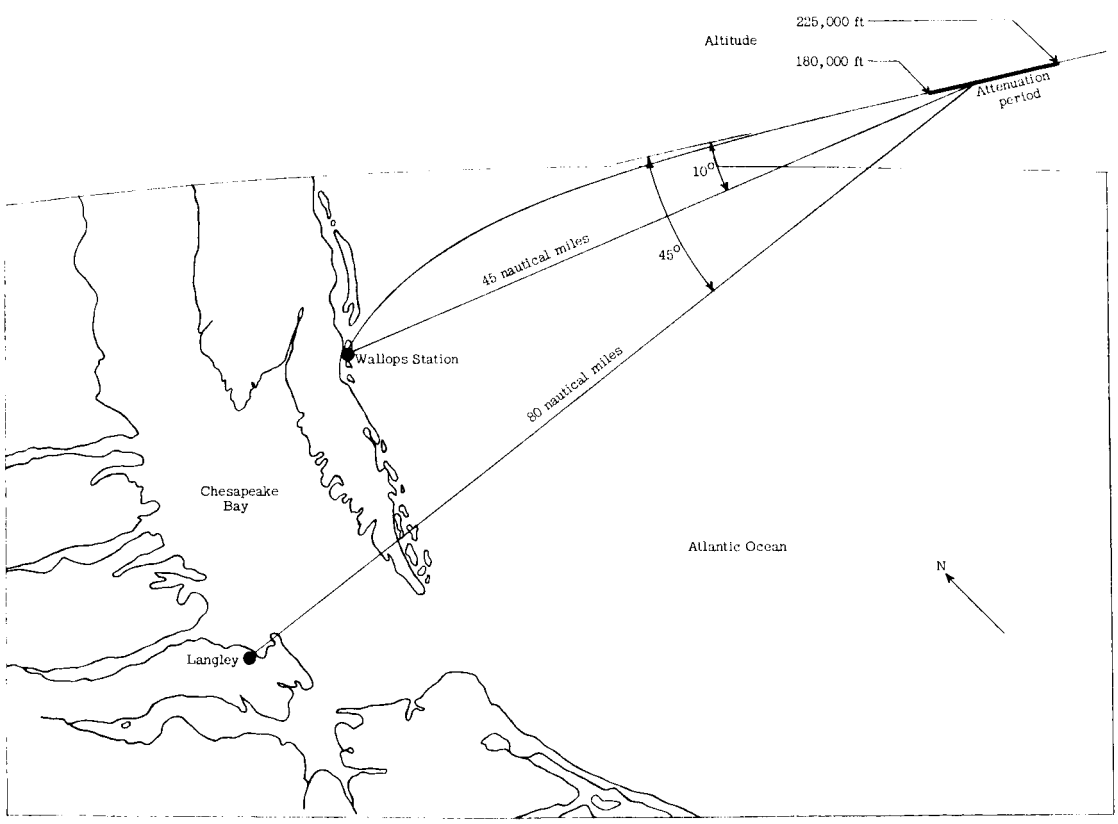

Figure 5.- Ground tracking range used in conjunction with ST-8 camera experiment.

during the attenuation period. Since the camera photographs both ignition and burnout of the second stage, the film can be easily correlated with the ground station data.

FLIGHT CAMERA EQUIPMENT AND OPERATION

Flight Camera

A modified gunsight camera was used in this experiment. The shutter assembly, which had to be modified to withstand the flight environment of the Scout vehicle, was a circular disk with a 36° open segment. The camera was designed to operate at 14.5 frames per second, which resulted in an exposure time of 1/145th of a second.

The lens was designed to withstand loadings up to 50g. It was a 9-element retro-focus design with an equivalent focal length of 0.1655 inch and a 110° field of view. The relative aperture was f/1.5 and the focus was set at infinity. The entire lens assembly was watertight.

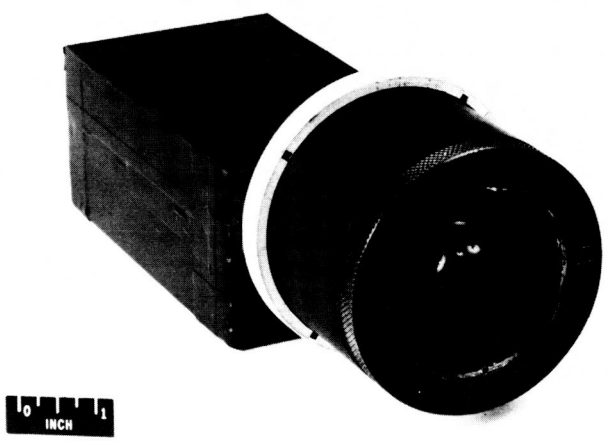

L-63-2137
Figure 6.- Photograph of camera flown on Scout ST-8.

The flight camera, including the lens assembly, is shown in figure 6. To increase the dynamic exposure range, a neutral density filter (density, -1.00; percent transmittance, -10) was placed over one-half the lens to reduce the exposure in that portion of the field. A thin-based color film was used to allow 180 feet to be loaded into the camera.

Pod Description

The camera was flown in a recoverable pod developed at the Langley Research Center. The pod is an 8-foot half-cylinder constructed of fiberglass cloth impregnated with epoxy resin. The pod was attached to the forward end of the second stage as shown in figure 2. The pod was self-contained and electrically independent of the launch vehicle.

Details of the pod are shown in figure 7. The camera was located in the lower end behind a fused quartz window. A SARAH radio beacon for use in the recovery was located in the camera compartment. The forward sections contained flotation material, a parachute, battery packs, separation devices, and a timer.

Since it was not possible to tilt the camera or lens assembly, a desired 90° field of view was obtained by placing a mirror in front of the lens (see

fig. 7) to recover that portion of the field of view lost on the vehicle side. The mirror and the neutral density filter created the four-quadrant film frame illustrated in figure 8. The left-hand side of the circle is the 0° to 45° portion measured from the center to the left. The firing direction of two of the control jets is indicated. The rectangular area on the right-hand side is the mirror image or 45° to 90° portion measured from the center to the right. The crosshatching indicates that part of the field affected by a neutral density filter.

Operation

By using a fly away umbilical the camera was turned on at -5 seconds and ran until +120 seconds to cover the burning of the first- and second-stage motors. At 120 seconds a timer contact closed and that portion of the pod below station 15.8 (fig. 7) was ejected from the vehicle. The ejection was accomplished by pyrotechnic release of a helical spring which gave the pod a rearward and lateral velocity component. The pod followed a ballistic trajectory to 135 miles altitude and then reentered the atmosphere. Reentry velocity was about 9,000 feet per second. At 20,000 feet a parachute was barometrically deployed to give the pod a water-impact velocity of 60 feet per second. Upon water entry a salt-water-actuated mechanism allowed the antenna to extend and the radio beacon guided the recovery team to the impact point.

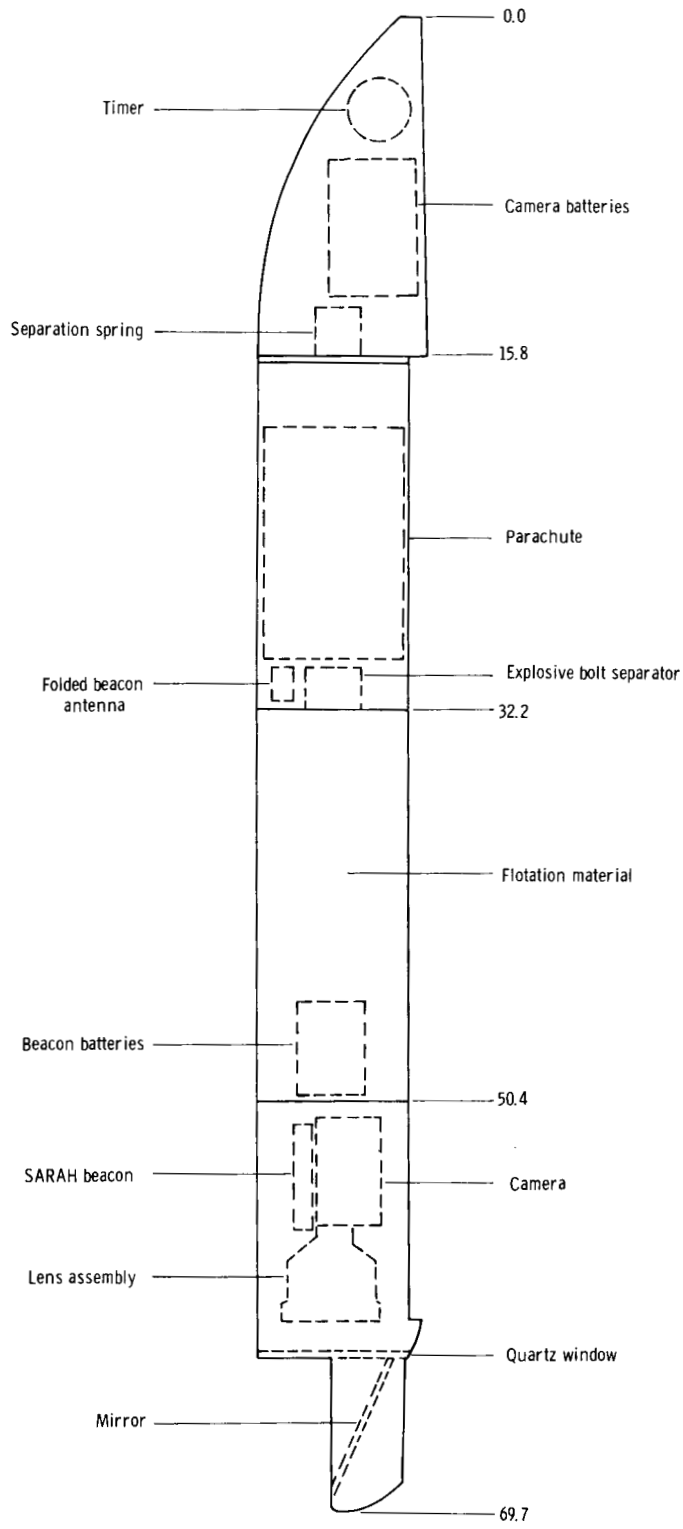

Figure 7.- ST-8 recoverable camera pod.

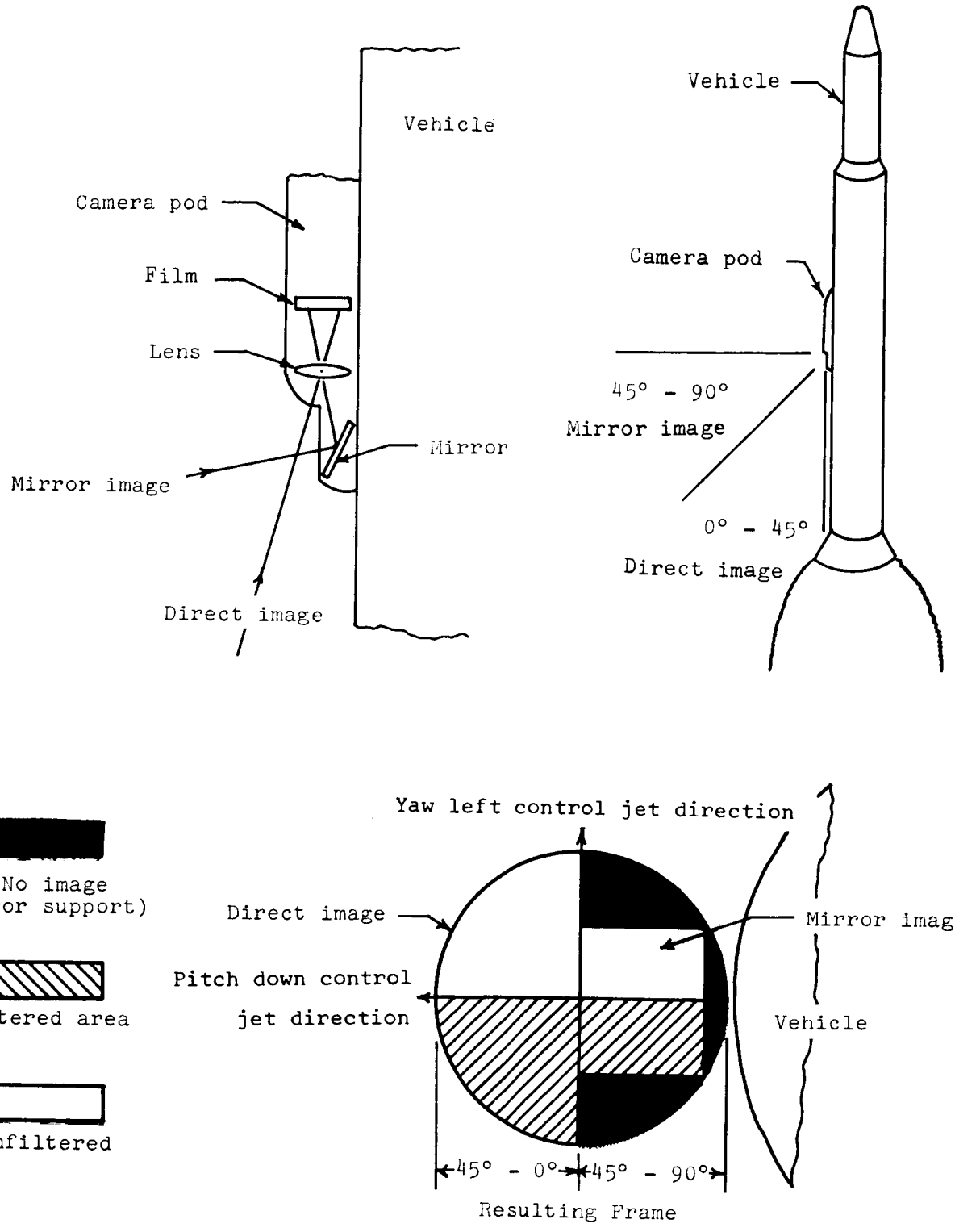

Figure 8.- Frame description for ST-8 flight camera.

RESULTS AND DISCUSSION

A motion-picture film supplement, an expanded-time copy of the original flight film, has been prepared and is available on loan. A request card form and a description of the film will be found at the back of this paper.

Vehicle and Camera Operation

Second-stage motor operation was normal and changes in vehicle attitude were negligible. Figure 9 shows vehicle altitude and velocity during this period. Camera pod operation, ejection, reentry, and recovery were normal; the film was returned in excellent condition.

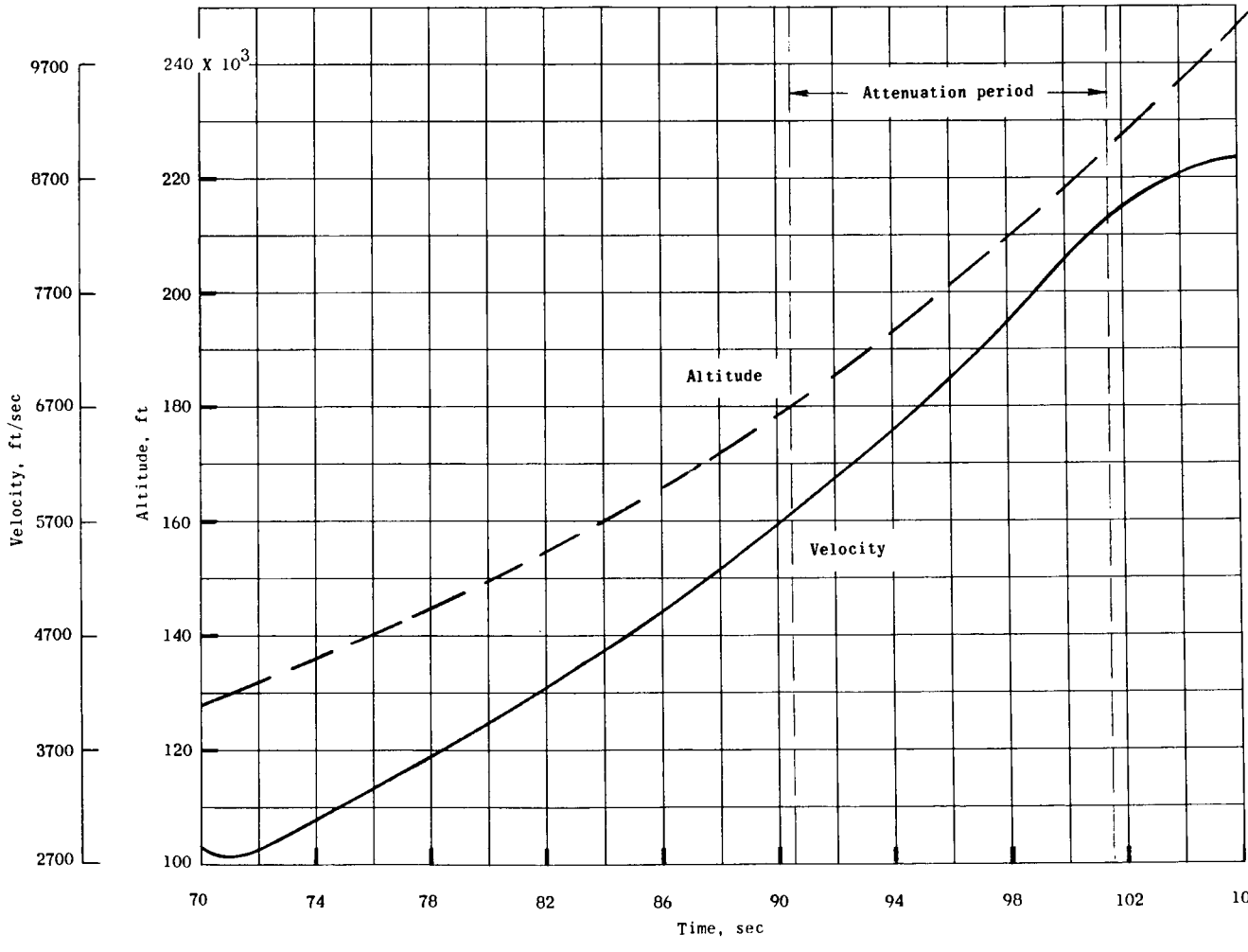

Figure 9.- Trajectory during second-stage motor burning.

Film Analysis

Because of uncertainties in expected available light and size of exhaust free jet, a filter and a mirror were employed to divide the film frame into four quadrants having different exposures and fields of view. In the recovered film the upper left-hand quadrant was found to show the desired information; therefore, only this portion is presented. Orientation of the camera with respect to the exhaust and the resulting "clear" quadrant are shown in figure 10. Also shown in the same figure is a single frame illustrating the appearance of the exhaust shortly after motor ignition at 71.2 seconds.

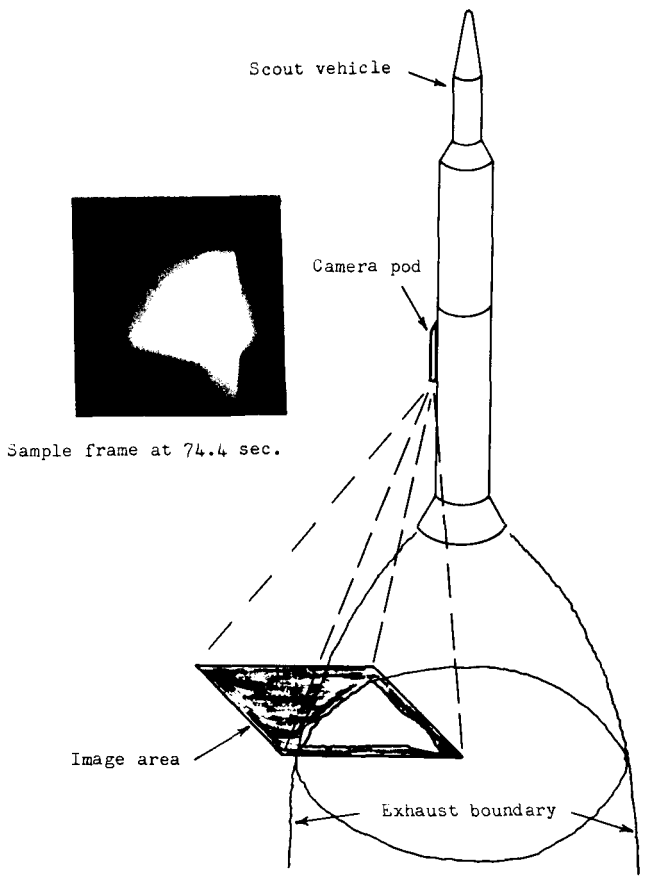

Figure 10.- Orientation of the camera with respect to the exhaust and sample film frame.

Important events from the film are illustrated by reproductions of the original film frames in figure 11. Although the original 16-millimeter color film shows the events very clearly, the necessary processing for the black and white reproductions for this publication resulted in some loss of detail; however, a copy of the original film, expanded in time by multiple framing techniques, is available on loan.

Sequence (a) of figure 11 (see figures for event times) is four consecutive frames showing the formation of an unusual "luminous ring" on the periphery of the exhaust image. The ring appeared at 90.7 seconds at 181,000 feet, as seen in the fourth frame. Initially, two rings were evident; however, they quickly merged into a single ring. There are two areas of luminosity: the ring and the "undisturbed cone" of the rocket exhaust.

Figure 11(b) shows ring removal in the direction of the pitch-down control jet. In figure 11(c), which shows both the yaw-left and pitch-down jets firing simultaneously, the ring is almost completely gone. In each of these sequences, only the ring is disturbed; the inner luminous area is unaffected. The three-frame sequence, also consecutive, in figure 11(d) shows the pitch-down jet firing and again a portion of the ring disappears. The radius of the ring is larger here than in previous sequences because of the rarer atmosphere. Figure 11(e) shows the ring as it disappears during tail off.

(a) Ring formation. 90.7 sec.

(b) Pitch control jet effect on ring. 92.7 sec.

Figure 11.- Significant frames from recovered flight film.

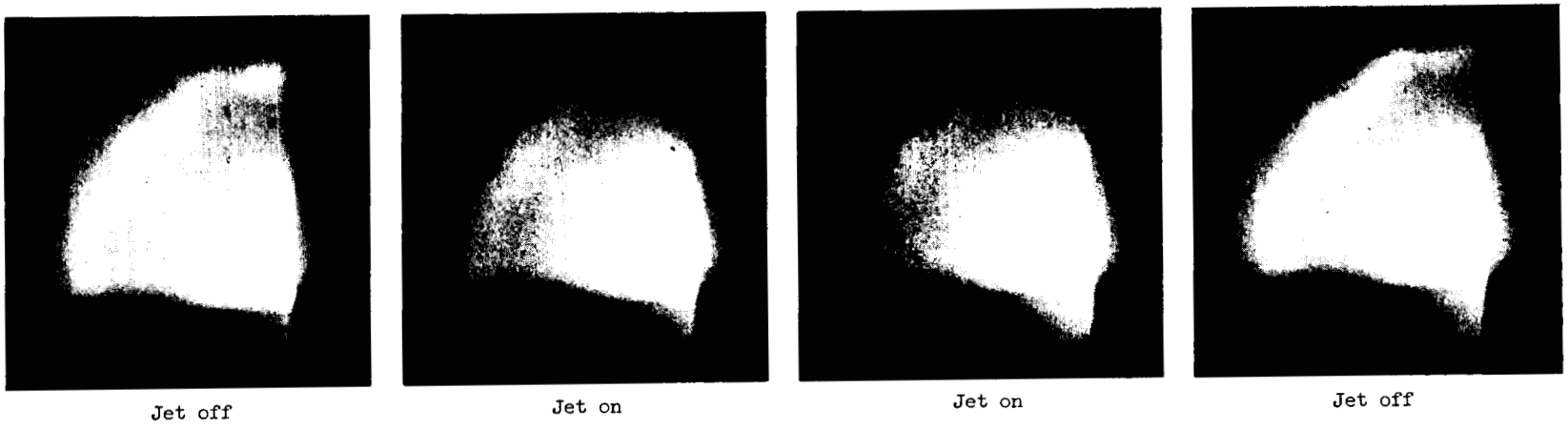

(c) Combined pitch and yaw control jet effect on ring. 95.9 sec.

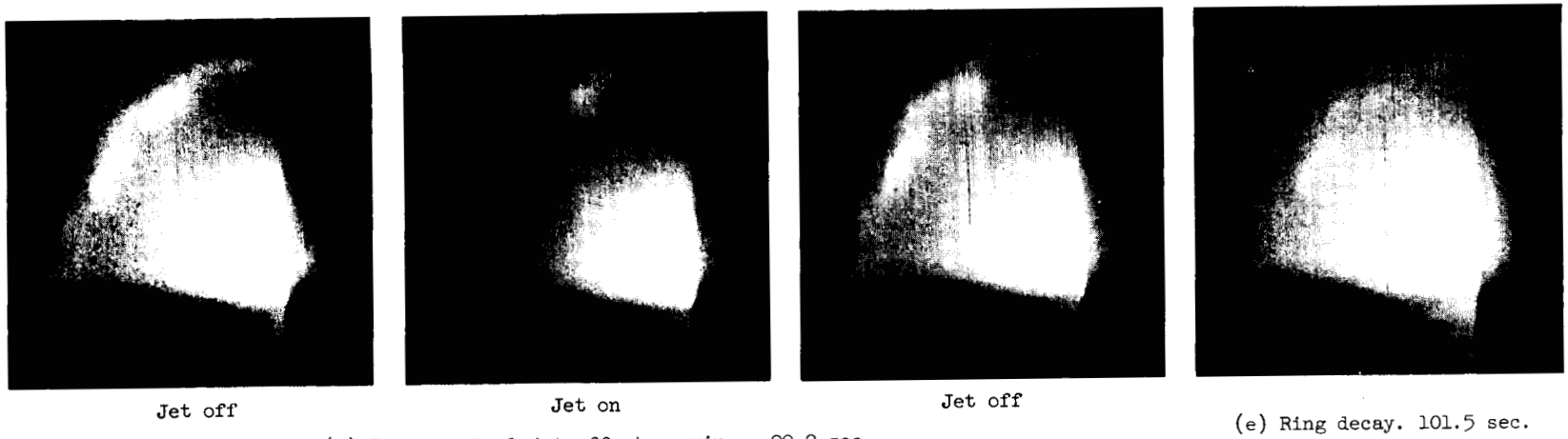

(d) Pitch control jet effect on ring. 99.2 sec.

(e) Ring decay. 101.5 sec.

Figure 11.- Concluded.

Tracking Station Observations

Telemetry signal interference, similar to that reported in reference 1, was observed at both tracking stations during second-stage burning. The effect began 90.7 seconds after launch, at 181,000 feet, and continued to 101.9 seconds, at 225,000 feet, during the tail-off portion of motor burning. The aspect angles from the stations to the vehicle during this period are shown in figure 12.

At the NASA Wallops Station, attenuation was observed on all three telemetry signals which reached a maximum of 20 decibels. Actuation of the control jets coincided with signal recovery. Wallops Station telemeter records during the period of interest are shown in figure 13.

Langley records are shown in figure 14. Attenuation was observed on the transition section telemetry signal only; the attenuation was 20 decibels at times. Signals from the two payload telemetry systems, however, were enhanced as much as 5 decibels at times. Again, signal recovery was coincident with control jet actuation. Telemetered information from the directional couplers in the payload antenna systems indicated no change in the voltage-standing-wave-ratio values during this period.

Correlation of Film and Signal Strength Data

The formation of the luminous ring observed on the film coincides exactly with the onset of pronounced signal interference at the ground stations. Each time a control jet is actuated and a portion of the ring disappears, signal recovery occurs.

Rocket Exhaust Plasma

The adverse effect of a rocket exhaust on radio signals is due to the presence of free electrons in the exhaust. These electrons and other ionized particles constitute a plasma which absorbs and reflects electromagnetic energy. Reference 6 describes some of the complex processes by which the electrons are generated. They include: (1) the primary combustion process in the combustion chamber, (2) a secondary combustion called afterburning which occurs on the exhaust surface, and (3) the ablation and subsequent ionization of the vehicle airframe and rocket nozzle.

References 7 and 8 describe the interaction of electromagnetic energy with the exhaust plasma. The absorptive and reflective properties of the plasma conductor depend on the electron density, the electron collision frequency, and the radio signal frequency. When the collision frequency is lower than the radio signal frequency, as would occur for low gas density, the interaction properties can be determined by the parameter f_p/f, where f_p is the plasma frequency and is porportional to the electron density according to the approximate relation

$$f_p \approx 10^4 \times (\text{electrons/cubic centimeter})^{1/2}$$

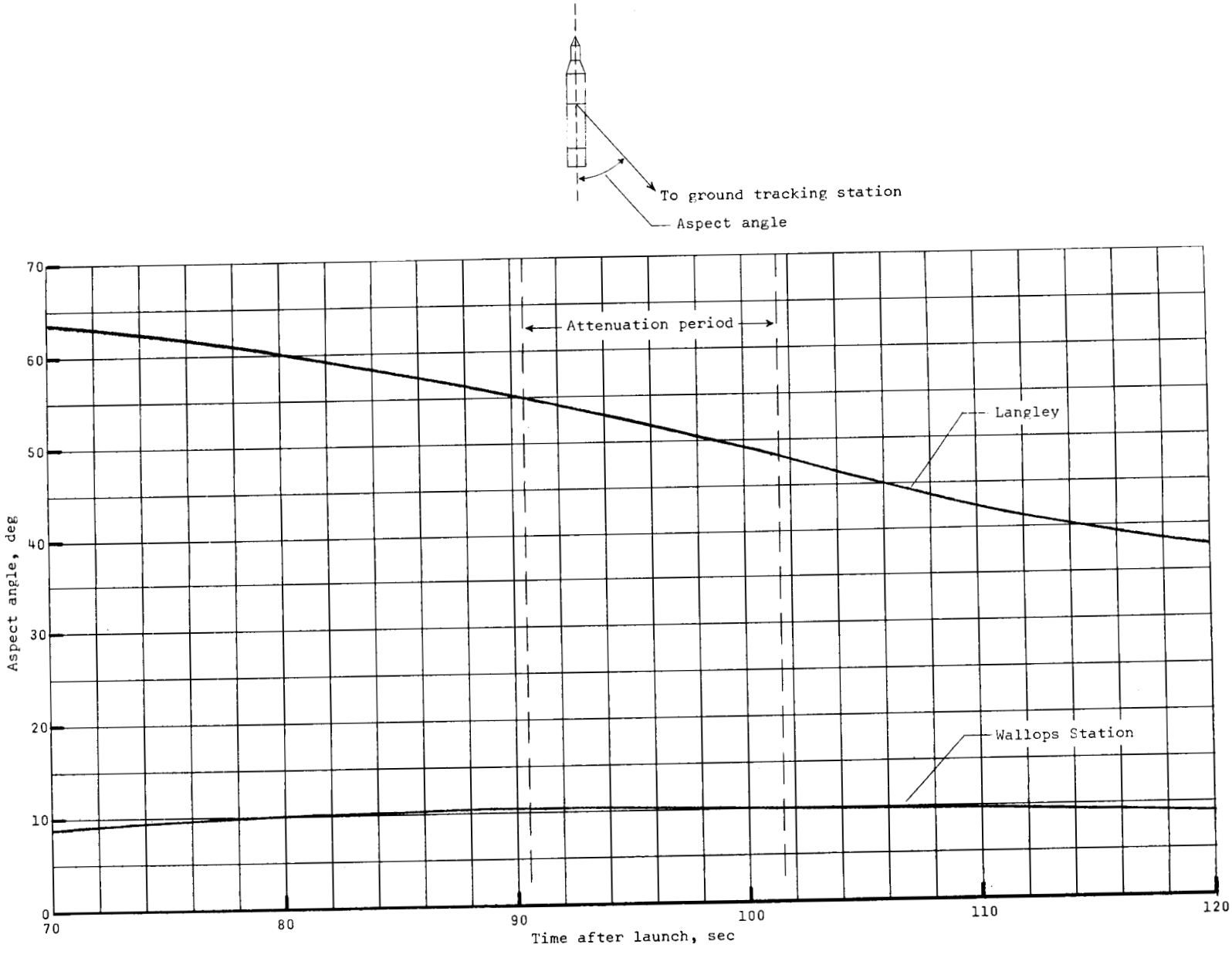

Figure 12.- Vehicle-to-tracking-station aspect angles during ST-8 second-stage motor operation.

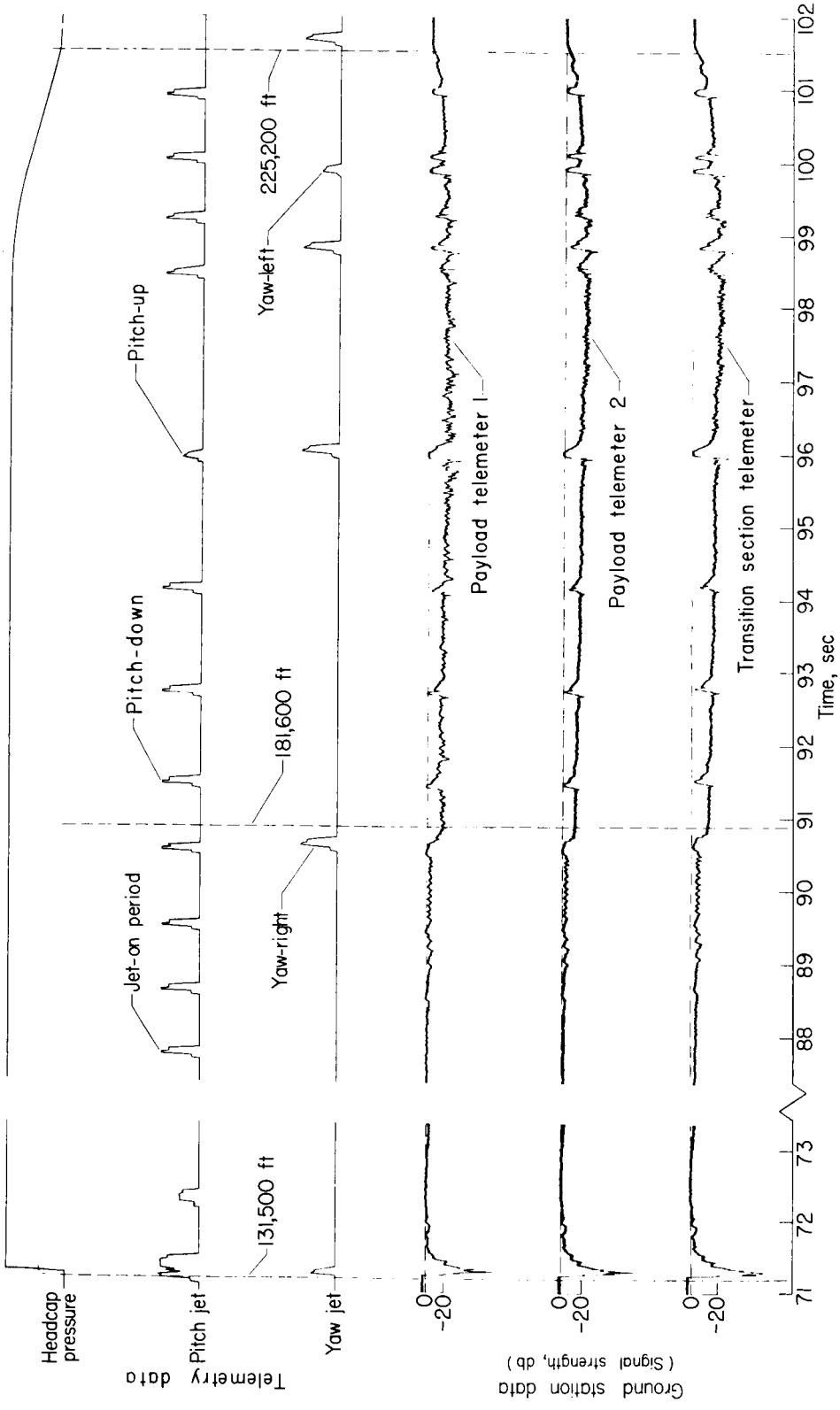

Figure 13.- Telemetry and signal strength data from the Wallops tracking station.

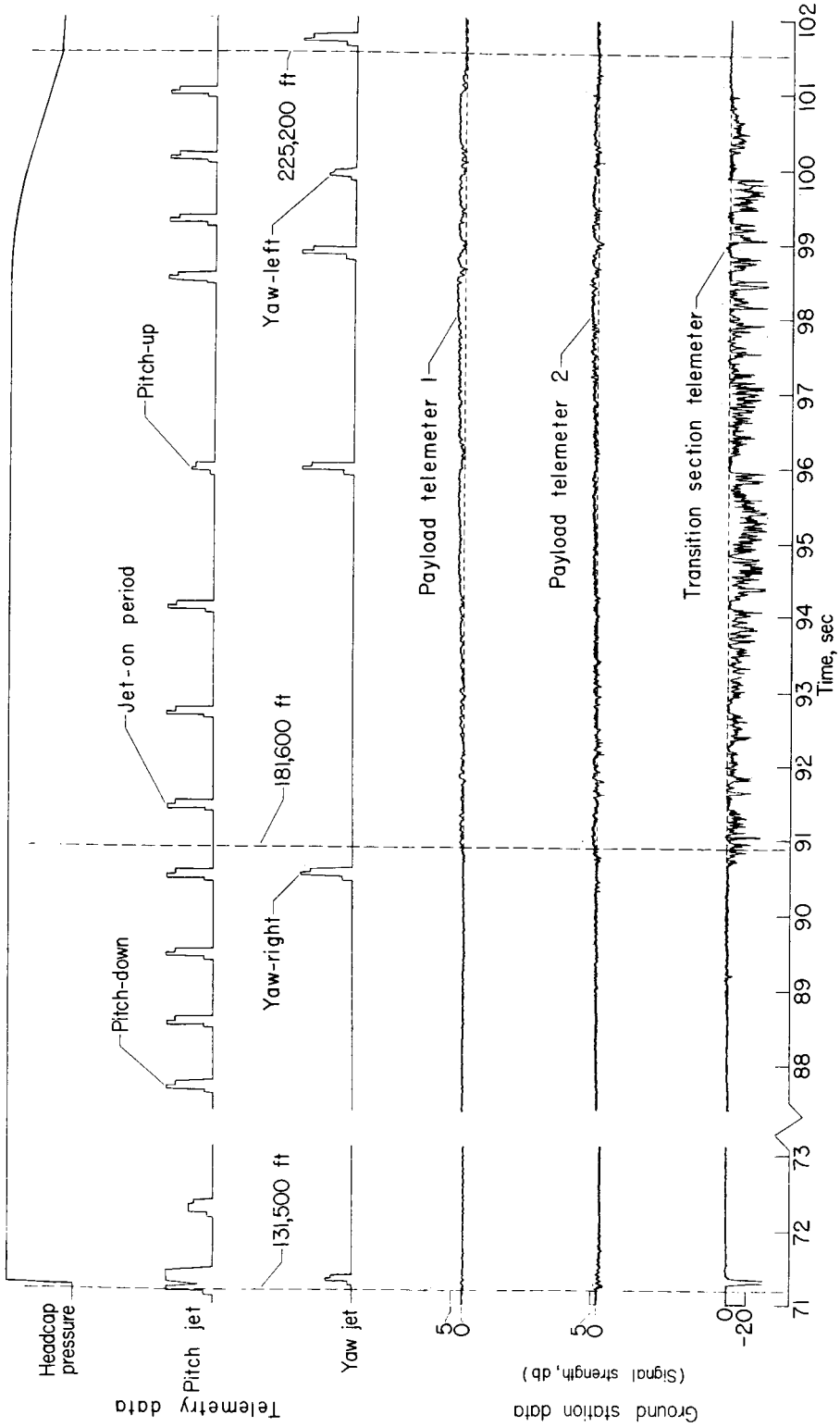

Figure 14.- Telemetry and signal strength data from the Langley tracking station.

and f is the signal frequency in cycles per second. When f_p/f is greater than 1, the plasma is defined as "overdense" and pronounced absorption and reflection will occur. If f_p/f is much less than 1, the plasma is "underdense" and is transparent to the radio signal. This latter point is the basis for the use of higher frequencies to avoid the attenuation problem.

Attenuation and Recovery Phenomenon

The Scout exhaust phenomenon was first observed on the initial Scout firing as reported in reference 1. It was suggested that the attenuation was caused by plasma on the surface of the exhaust as a result of afterburning. Signal recovery was attributed to cooling of the exhaust flow field interface by exhaust products of the control jets and subsequent removal of electrons by recombination and attachment processes. High-temperature air in the separated flow region around the vehicle and electrons in the ionosphere were suggested as possible contributors to surface exhaust plasma. One purpose of the camera experiment on the Scout vehicle was to substantiate these conclusions.

Luminous ring.- The photographic record of the Scout second-stage exhaust clearly shows changes in structure that correspond with recorded changes in ground-signal strength data. The luminous ring, which corresponds with the attenuation period, supports the exhaust surface afterburning hypothesis suggested in reference 1. Figure 15 is a plot of the angular measurement of the growth of the exhaust and luminous ring. The ring appears to be separate from the "undisturbed inner cone," the luminosity and size of which remain relatively constant. To examine the conditions attendant to ring formation, it is necessary to examine the Scout flow field.

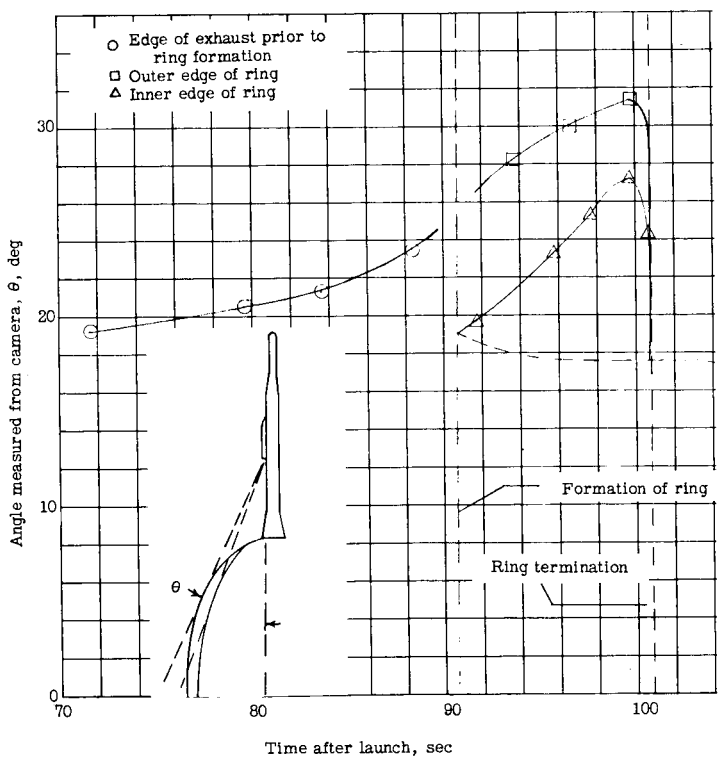

Figure 15.- Angular measurements of exhaust and "ring" from the recovered flight film.

Exhaust-flow field interaction and afterburning.- Reference 9 describes the expansion of a rocket exhaust at high altitudes and shows that two of the factors that affect the size are the ratio of the jet exit pressure to ambient pressure and the vehicle Mach number. The exhaust size will

increase with increasing pressure ratio while increasing Mach number will tend to compress the exhaust. The ratio of jet pressure to free-stream pressure during the attenuation period is shown in figure 16. Figure 17 shows the Mach and Reynolds numbers during the same period.

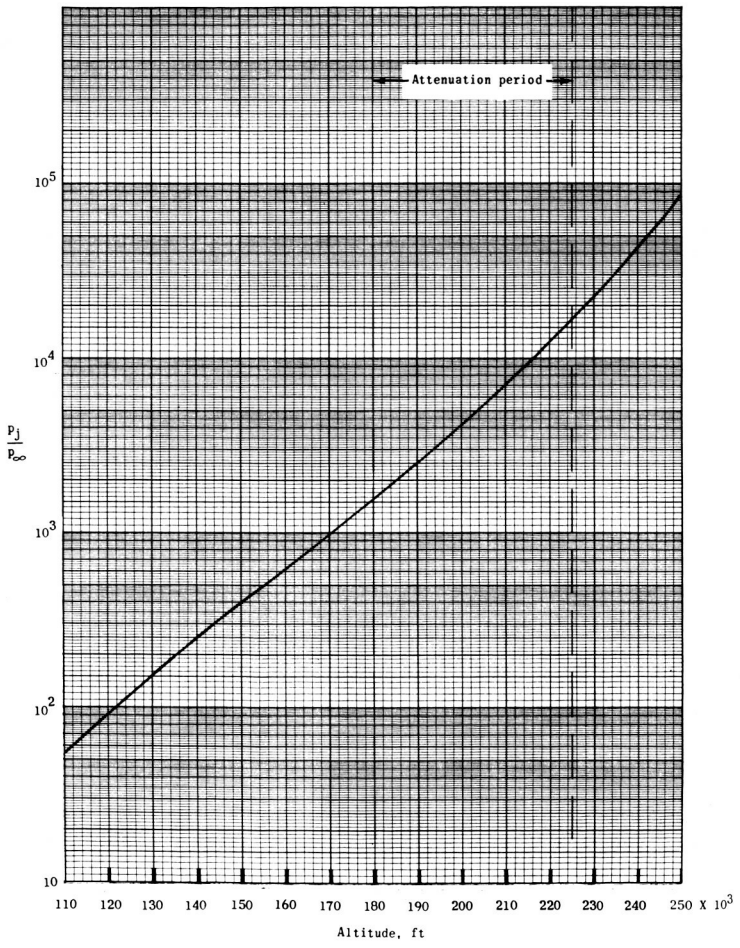

Figure 16.- Ratio of jet-exit pressure to free-stream pressure during ST-8 second-stage motor operation.

References 10 and 11, which report on the effects of free jets on vehicle stability, indicate that a large free jet causes the free stream to deflect, and thereby creates a shock wave which interacts with the boundary layer of the vehicle. Because of this interaction, flow separation can occur along the vehicle surface. For Reynolds numbers less than 10^6, the boundary layer is probably laminar and, hence, more susceptible to separation. The separated flow re-attaches to the exhaust free jet at some distance from the vehicle and creates on the free-jet surface a turbulent mixing region. This flow-exhaust interaction is shown in the schlieren photograph in figure 18 which was taken from reference 11.

Figure 19, which is based on information from references 9 to 12, summarizes the principal features of the exhaust free jet and vehicle flow field interaction for the Scout during the attenuation period. The primary characteristics are the following: (1) large expanded exhaust free jet and the resulting separated-flow region; (2) turbulent mixing region beginning at the attachment of the separated boundary downstream of the nozzle; and (3) shock waves in the flow field such as the bow shock, the shock off the separated region, the shock off the jet boundary, and the internal jet shock.

In the mixing region, hydrogen and carbon monoxide exhaust gases combine with heated air from the supersonic flow field and even higher temperature air from the separated flow field and are believed to cause afterburning. Associated with this afterburning are thermal and chemical ionization processes which create a sheath of electrons on the jet surface. (See ref. 6.) As explained in reference 7, this layer of electrons can cause attenuation and reflection of electromagnetic energy.

The end of afterburning and associated attenuation occurs during tail off, when less gas is exhausting and the extreme altitude provides insufficient oxygen for external combustion. The onset of afterburning is more difficult to explain because a detailed analysis of exhaust conditions is not available. Some of the complex factors that affect the limits of inflammability are fuel-to-oxidizer ratio, temperature, pressure, and flame size, as described in reference 13. Conditions which are conducive to combustion have been outlined and the actual formation of the luminous ring is evidence that combustion did occur.

Other possible excitation modes.- Photoionization by sunlight can be discounted since this launch occurred at night. Ionization from the ionosphere D region, suggested in reference 1, was probably negligible during this flight since electron density in this region is severely reduced at night. Ablation of the vehicle heat protection system can be neglected since maximum aerodynamic heating occurred at altitudes lower than that of the attenuation period. Shock interaction resulting from the impingement of the free-stream flow on the exhaust (fig. 19) may cause some excitation and ionization.

Antenna pattern change.- Observation of attenuation at low aspect angles and enhancement at large aspect angles suggests that an effective change in the antenna radiation pattern occurred as a result of the exhaust plasma. A highly reflective exhaust boundary would cause this effect and

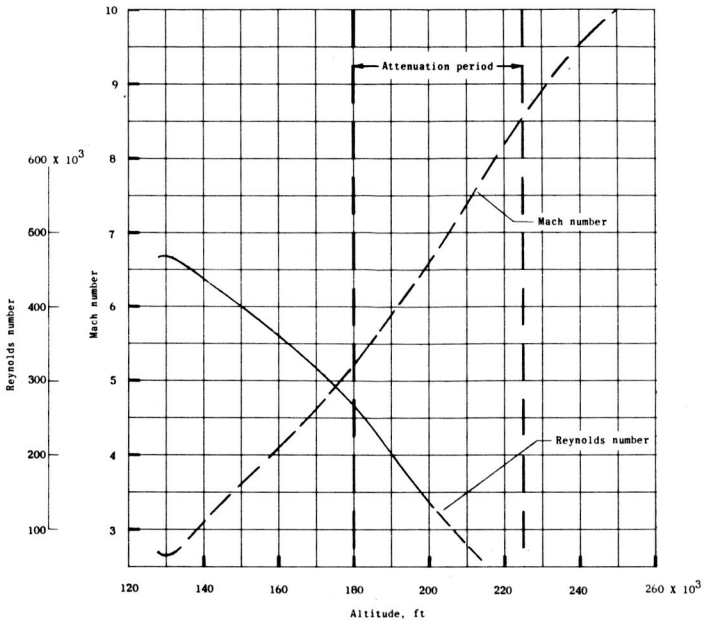

Figure 17.- Reynolds number (based on 40-foot length) and Mach number during ST-8 second-stage motor operation.

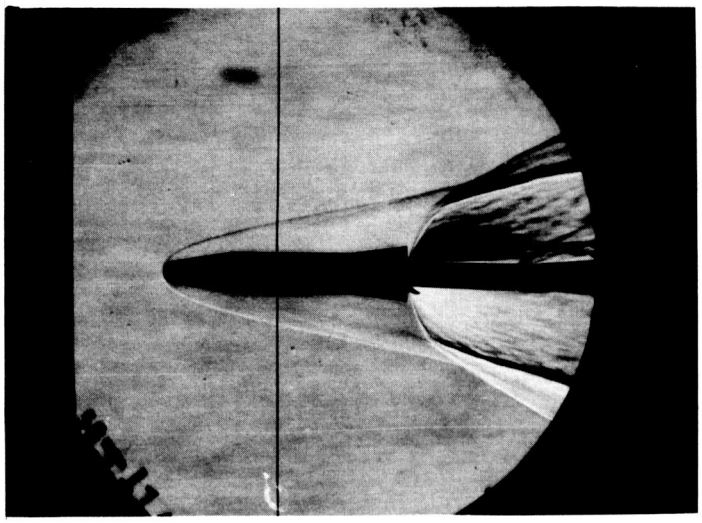

L-63-4701

Figure 18.- Schlieren photograph of a model in wind tunnel. (From ref. 11.)

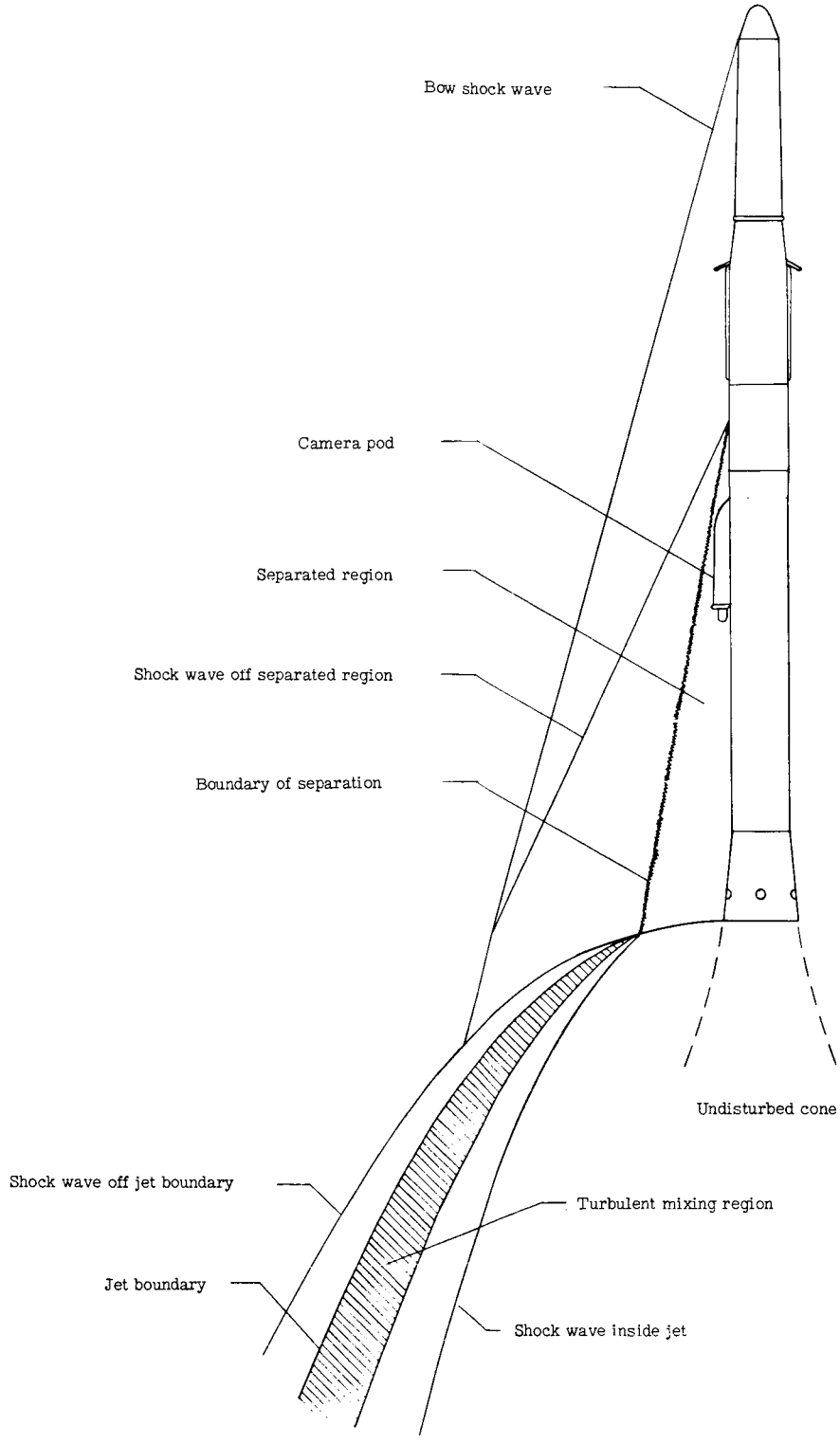

Figure 19.- Typical flow field for ST-8 during attenuation period.

is consistent with the concept of an overdense plasma. (See fig. 20).

Metal cones simulating an overdense plasma were attached to a 1/10-scale model of the Scout and the change in antenna pattern was observed to be in agreement with flight results. There may be a possibility of reflection from the exhaust surface when the plasma is slightly underdense. This would be the case when the angle of incidence between the electromagnetic radiation and the plasma surface is large. (See ref. 14.)

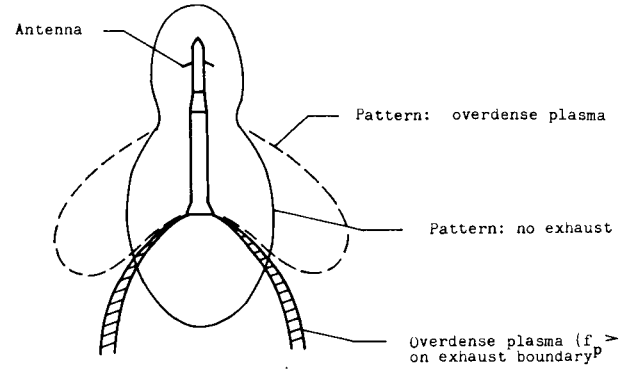

Figure 20.- Concept of antenna pattern change due to overdense plasma on surface of exhaust.

The possibility of antenna breakdown or antenna effects causing the observed attenuation is discounted because of the observed enhancement at the down-range station and the fact that the telemetered data from the directional couplers in the payload telemetry antennas showed no change during the attenuation period.

The signal-strength record from the Langley Station illustrates the effect of antenna location. Signals from the transition section antenna, which is approximately 10 feet closer to the exhaust than the payload antennas, show attenuation, while those from the payload show enhancement. This difference in signals indicates that analyses of the aspect angle effect of rocket exhausts must take into account the position of the vehicle antenna with respect to the exhaust.

The aspect angle to the Wallops Station, compared with angle data from the film, indicates that signals to that station were passing through the exhaust prior to the formation of the ring. Pronounced attenuation, however, appeared only after the ring had formed. Analysis of film angle data compared with the Langley aspect angle indicates that the Langley station was not looking through the exhaust during the period of attenuation, and thus the concept of antenna pattern change is supported.

Signal recovery.- As has been described in the foregoing, control jet operation causes signal recovery during periods of observed attenuation. The film, moreover, revealed that control jet operation caused elimination of a portion of the luminous ring, identified as afterburning. The necessary conclusion, therefore, is that the products of the hydrogen peroxide control jet (water vapor and oxygen) quench afterburning and eliminate attenuation by shielding the flow field from the exhaust gases and cooling the mixing region. The possibility of other materials being more efficient should be investigated.

Attachment and recombination were discussed in reference 1 as possible means of electron elimination. Adequate analysis of the importance of these processes is not possible because of a lack of knowledge of conditions in the afterburning region. However, their effects should not be discounted.

The general concept of externally injecting materials to eliminate exhaust-induced attenuation should also be thoroughly explored because of its application where changes in propellant composition, relocation of ground tracking stations, or changes in communication link frequencies are not possible.

CONCLUSIONS

A recoverable camera was flown on a NASA Scout vehicle to photograph the exhaust of the second-stage motor during an anticipated period of unusual radio frequency signal attenuation. Analysis of the recovered film and signal strength data indicates the following:

1. A luminous ring which appears in the film is believed to be afterburning on the exhaust surface as a result of a mixing interaction with the vehicle flow field.

2. Electrons created by ionization processes in the afterburning sheath cause attenuation and reflection of radio frequency energy.

3. Decomposed hydrogen peroxide from the control jets quenches the afterburning and signal recovery occurs.

4. The observed radio frequency interference can be explained in terms of an effective change in vehicle antenna pattern.

5. The lack of change in vehicle antenna voltage standing wave ratio indicates that antenna breakdown did not occur.

6. The aspect-angle dependence on attenuation is affected by the position of the vehicle antenna relative to the exhaust.

7. The external injection of materials to eliminate exhaust-induced attenuation appears promising as a solution especially when other techniques such as changes in propellant composition, relocation of ground stations, and changes in communication link frequencies are not practical. Additional study to determine the range of applicability and the choice of material is indicated.

Langley Research Center,
National Aeronautics and Space Administration,
Langley Station, Hampton, Va., June 20, 1963.

REFERENCES

1. Sims, Theo E., and Jones, Robert F.: Rocket Exhaust Effects on Radio Frequency Propagation From a Scout Vehicle and Signal Recovery During the Injection of Decomposed Hydrogen Peroxide. NASA TM X-529, 1961.

2. Balwanz, W. W., and Stine, P. T.: The Plasmas of Missile Flight - Analysis of the Polaris A2X Signal Absorption. NRL Rep. 5636, U.S. Naval Res. Lab., July 24, 1961.

3. Fetner, E. M., and Hoffmann-Heyden, A. E.: R-F Interference by Solid Fuel Rocket Exhausts. AFMTC-TR-61-10 (Contract No. AF08(606)-3413), Air Force Missile Test Center, U.S. Air Force, Sept. 1, 1961.

4. Mayhue, Robert J., Compiler: NASA Scout ST-1 Flight-Test Results and Analysis, Launch Operations, and Test Vehicle Description. NASA TN D-1240, 1962.

5. Sims, Theo E., and Jones, Robert F.: Flight Measurements of VHF Signal Attenuation and Antenna Impedance for the RAM A1 Slender Probe at Velocities Up to 17,800 Feet Per Second. NASA TM X-760, 1963.

6. Calcote, H. F., and Silla, H.: Radar Attenuation in Solid Propellant Rocket Exhausts. Bull. 18th Meeting JANAF-ARPA-NASA Solid Propellant Group, Vol. III, June 1962, pp. 3-50.

7. Altshuler, S., Moe, M. M., and Molmud, P.: The Electromagnetics of the Rocket Exhaust. GM-TR-0165-00397, Space Technology Labs., Inc., June 15, 1958.

8. Huber, Paul W., and Nelson, Clifford H.: Plasma Frequency and Radio Attenuation. Proceedings of the NASA-University Conference on the Science and Technology of Space Exploration, Vol. 2, NASA SP-11, 1962, pp. 347-360. (Also available as NASA SP-25.)

9. Love, Eugene S., Grigsby, Carl E., Lee, Louise P., and Woodling, Mildred J.: Experimental and Theoretical Studies of Axisymmetric Free Jets. NASA TR R-6, 1959. (Supersedes NACA RM L54L31 by Love and Girgsby, RM L55J14 by Love, RM L56G18 by Love, Woodling, and Lee, and TN 4195 by Love and Lee.)

10. Falanga, Ralph A., Hinson, William F., and Crawford, Davis H.: Exploratory Tests of the Effects of Jet Plumes on the Flow Over Cone-Cylinder-Flare Bodies. NASA TN D-1000, 1962.

11. Hinson, William F., and Falanga, Ralph A.: Effect of Jet Pluming on the Static Stability of Cone-Cylinder-Flare Configurations at a Mach Number of 9.65. NASA TN D-1352, 1962.

12. Boynton, F. P.: The Afterburning of Rocket Engine Exhausts. GM-60-0000-13732, Proc. of Conf. on Ions in Flames, Space Technology Labs, Inc., 1960.

13. Gaydon, A. G., and Wolfhard, H. G.: Flames, Their Structure, Radiation and Temperature. Second Ed., Rev., Chapman & Hall Ltd. (London), 1960.

14. Graf, K. A., and Bachynski, M. P.: Transmission and Reflection of Electromagnetic Waves at a Plasma Boundary for Arbitrary Angles of Incidence. Canadian Jour. Phys., vol. 39, no. 11, Nov. 1961, pp. 1544-1562.